PHYSICAL REVIEW B VOLUME 27, NUMBER 6 15 MARCH 1983

Acoustic saturation in a glass at low temperatures

J. E. Graebner, L. C. Allen, B. Golding, and A. B. Kane
Bell Laboratories, Murray Hill, New Jersey 07974
(Received 21 October 1982)

An experimental and theoretical study of nonlinear acoustic propagation in a typical glass, fused silica, is presented, at frequencies near 1 GHz and temperatures below 1 K. The data are interpreted within a general framework of pulse propagation in an inhomogeneously broadened two-level absorber. Numerical solutions are compared with the temperature and pulse-width dependence of the critical saturation intensity, as well as with saturation recovery experiments. The data are described by a linewidth T_2^{-1} of the intrinsic tunneling states that agrees with lifetimes obtained from phonon echo experiments. The distribution of relaxation times T_1 which emerges from the analysis of saturation recovery experiments is also understandable within the tunneling model. An improved estimate for the longitudinal deformation potential is $\gamma_L = 2.0$ eV. For $T < 0.1$ K, the behavior of the pulse velocity is indicative of a coherent propagating mode, i.e., self-induced transparency.

I. INTRODUCTION

The two-level tunneling model of a glass was developed[1,2] to explain the nearly universal properties of disordered materials[3,4] at temperatures below approximately 1 K, namely, the large specific heat varying roughly as T and the small thermal conductivity $\sim T^2$. Both properties are explained by assuming the existence of many intrinsic two-level configurational states which consist of unspecified atoms or groups of atoms. The roughly constant density of states as a function of energy splitting that is expected in a glass accounts for the quasilinear specific heat, while a strong coupling to phonons through a resonant scattering process explains the small thermal conductivity.

The first prediction[2] of the tunneling model to be verified experimentally was the phenomenon of acoustic saturation. This observation[5,6] confirmed the idea that only the two lowest energy levels are needed to describe the dynamics of these systems. The formal equivalence of the quantum mechanics of all two-level systems has been exploited by borrowing analytical techniques from the fields of magnetic resonance[7] and coherent optics.[8,9] Acoustic propagation in a glass at low temperatures is closely related to optical pulse propagation in a medium containing two-level atoms with an extremely broad inhomogeneous line shape.

A variety of acoustic phenomena[10,11] has been investigated: the unsaturated (low-intensity) attenuation, the critical intensity needed for saturation, the saturated linewidth, the recovery of the states from saturation, and the coherent acoustic phenomenon known as phonon echoes, analogous to photon echoes. The present work is an extension of a previous investigation[12,13] of the saturation threshold and of the recovery of equilibrium after saturation. The interpretation of saturation data is sensitive to which regime one is in (e.g., steady-state or pulse), a fact which has not always been taken into account properly in several recent investigations. Therefore, our purpose is twofold: (1) to describe, in rather general terms, acoustic propagation under a wide variety of experimental conditions, and (2) to apply these results to our data in a glass at low temperatures in order to extract relaxation times and coupling strengths.

A brief outline of the two-level tunneling model is presented in Sec. II, followed by an analysis of the interaction of the two-level systems and an acoustic wave. Section III describes the numerical procedures used to simulate pulse propagation. The data are presented and analyzed in Sec. IV.

II. THEORY

A. Two-level tunneling model

Each two-level tunneling system in a glass is described by a double-well potential of asymmetry Δ and overlap energy $\Delta_0 = \hbar\Omega e^{-\lambda}$, where Ω is a typical zero-point energy in either well and $\lambda = (d/\hbar)(2mV)^{1/2}$. V is the barrier height, d is a generalized tunneling coordinate, and m is an effective mass of the two-level system. Tunneling through the potential barrier mixes the eigenstates of the two independent wells, resulting in an energy splitting

$$E=(\Delta^2+\Delta_0^2)^{1/2} . \tag{1}$$

The Hamiltonian for the system coupled to a long-wavelength strain e is

$$\begin{aligned} H&=H_0+H_1 \\ &=(E/2)\sigma_z-(M\sigma_x+\tfrac{1}{2}D\sigma_z)e(z,t) . \end{aligned} \tag{2}$$

M and D are the off-diagonal and diagonal coupling parameters and are related to the deformation potential $\gamma\equiv\partial\Delta/\partial e$ by

$$M=\frac{\Delta_0}{E}\gamma, \quad D=\frac{\Delta}{E}\gamma . \tag{3}$$

γ is averaged over the orientations of the two-level systems with respect to the strain tensor. The density of states $p(\lambda)$ is usually taken to be a constant, which leads to a roughly constant density of states n_0 per unit energy. In the language of optical or magnetic resonance, the roughly constant density of states in the vicinity of the pulse spectrum can be described as the center of an inhomogeneously broadened line of line shape given by the normalized function $g(\zeta)$, with $\zeta=\omega_0-\omega=(E/\hbar)-\omega$. $g(\zeta)d\zeta$ is then the fraction, of the total number N of states per cm^3, that lies between ζ and $\zeta+d\zeta$, with the normalization $\int g(\zeta)d\zeta=1$. It is convenient to write $g(\zeta)$ as a Lorentzian

$$g(\zeta)=\frac{1}{\pi}\frac{T_2^*}{1+(T_2^*\zeta)^2} , \tag{4}$$

which acts as a δ function when integrated over ζ. The appropriate definition for T_2^* is $\pi\hbar n_0/N$.

Equations (1) and (3) imply a distribution of coupling parameters M and D for different states with the same energy splitting. This, in turn, leads to a distribution of the one-phonon relaxation rate given by[1,14]

$$\begin{aligned} T_1^{-1}(E,\lambda)=&\left[\frac{\gamma_L^2}{c_L^5}+\frac{2\gamma_T^2}{c_T^5}\right]\frac{E^3}{2\pi\hbar^4\rho_0} \\ &\times\exp[-2(\lambda-\lambda_{\min})] \\ &\times\coth(E/2k_BT) , \end{aligned} \tag{5}$$

where subscripts L and T refer to longitudinal and transverse phonon polarizations, respectively, c is the acoustic velocity, ρ_0 is the mass density, and $\lambda_{\min}$ is the minimum value of λ for a given E, corresponding to the symmetric levels ($\Delta=0$). Under the assumption $p(\lambda)=$const, one can calculate the distribution of relaxation rates for any given value of E. Jäckle[14] finds, for instance,

$$p(r)=\frac{1}{2(1-r)^{1/2}r} , \tag{6}$$

where

$$r=T_1^{-1}(E,\lambda)/T_1^{-1}(E,\lambda_{\min}) .$$

In the analysis which follows, we assume a single-valued $T_1=T_{1(\min)}$ and defer until Sec. IV a discussion of the possible effects of a distribution of T_1's.

B. Basic equations of motion

Acoustic pulse propagation in this saturable medium is governed by the acoustic wave equation coupled with the acoustic equivalent of the Bloch equations which describe the local dynamics of the two-level systems. The general procedure has been outlined by Shiren[15] for the case of acoustic paramagnetic resonance, following an approach for the analogous optical case developed by McCall and Hahn[16] for self-induced transparency. A number of related calculations have been made.[17,18]

One can identify two contributions to the propagating stress: the usual term due to the restoring forces of the elastic medium, and a contribution R due to the motion induced in the configurational states. If we restrict ourselves to a plane wave of strain e and suppress tensor indices, the stress T is

$$T=\frac{\partial}{\partial e}(c^2\rho_0e^2/2+H)=c^2\rho_0e+R , \tag{7}$$

where H is given by Eq. (2) and ρ_0 is the mass density. Differentiation with respect to z of the basic force equation leads to a wave equation of the form

$$\frac{1}{c^2}\frac{\partial^2e}{\partial t^2}-\frac{\partial^2e}{\partial z^2}=\frac{1}{\rho_0c^2}\frac{\partial^2R}{\partial z^2} \tag{8}$$

for a plane strain wave traveling along the z direction, which we take to be

$$e(z,t)=e_0(z,t)\cos[\omega t-kz-\phi(z)] . \tag{9}$$

The envelope function $e_0(z,t)$ is a real quantity, $k=\omega/c$, and ϕ is a phase angle. The response of the system can be calculated from the quantum-mechanical equations governing the two-level tunneling states using a density-matrix approach. In terms of the density matrix ρ, the expectation value for R is

$$\langle R\rangle=N\,\mathrm{Tr}\left[\frac{\partial H}{\partial e}\rho\right] . \tag{10}$$

The elements ρ_{aa} and ρ_{bb} are, respectively, the fractional populations of the upper and lower states, while ρ_{ab} and $\rho_{ba}=\rho_{ab}^*$ are related to the complex elastic dipole moment. Only one of the two

counter-rotating strain components represented by (9) is effective in causing transitions. The matrix element $(H_1)_{ba}$, for example, in the rotating-wave approximation is

$$(H_1)_{ba} = -(e_0 M/2)\exp[i(\omega t - kz - \phi)] .$$

Transforming to the rotating coordinate system by means of

$$U = \begin{bmatrix} e^{-i\omega t/2} & 0 \\ 0 & e^{i\omega t/2} \end{bmatrix} \tag{11}$$

simplifies the Hamiltonian to

$$H' = \frac{1}{2}\begin{bmatrix} \alpha & -\beta \\ -\beta^* & -\alpha \end{bmatrix}, \tag{12}$$

where

$$\alpha = E - \hbar\omega - De_0\cos(\omega t - kz - \phi)$$

and $\beta = Me_0 e^{i(kz+\phi)}$.

The equation of motion of the transformed density matrix $\rho' = U^\dagger \rho U$ is given by

$$i\hbar\dot{\rho}' = [H', \rho'] , \tag{13}$$

where H' is the transformed Hamiltonian. Defining

$$u = \rho'_{ab}\exp[-i(kz+\phi)] + \text{c.c.}, \tag{14}$$

$$v = i\rho'_{ab}\exp[-i(kz+\phi)] + \text{c.c.}, \tag{15}$$

and

$$w = \rho'_{aa} - \rho'_{bb} , \tag{16}$$

one can write (13) in the form

$$\dot{u} = -\zeta v + \xi v - u/T'_2 , \tag{17}$$

$$\dot{v} = \zeta u - \xi u + (Me_0/\hbar)w - v/T'_2 , \tag{18}$$

and

$$\dot{w} = -(Me_0/\hbar)v - (w - w_0)/T_1 , \tag{19}$$

where w_0 is the equilibrium difference in occupation probabilities,

$$w_0 = -\tanh(\hbar\omega/2k_B T) ,$$

and

$$\xi = (De_0/\hbar)\cos(\omega t - kz - \phi) .$$

Equations (17)–(19) are the acoustic analog of the Bloch equations of magnetic resonance. Relaxation times T_1 and T'_2 have been introduced in the usual way. T'_2 is the phase memory time and T_1 is the time for thermal equilibrium. For convenience in what follows, we abbreviate T'_2 to T_2. The terms containing ξ result in a longitudinal coupling of the sound wave with the two-level systems which produces a high-frequency small-amplitude variation of the precession about the w axis. For pulses which are more than a few cycles in length, and particularly for states with strong off-diagonal coupling ($D \ll M$), the terms containing ξ may safely be ignored.

We can distinguish three regimes of pulse length τ with respect to T_1 and T_2.

(1) Coherent regime ($\tau \ll T_1, T_2$). Relaxation is unimportant in this regime and many coherent propagation effects are observable, such as phonon echoes, self-induced transparency, etc., in direct analogy with coherent optics.

(2) Intermediate regime ($T_2 < \tau < T_1$). Phase memory is lost during the pulse but populations are functions of z, t, and ζ.

(3) Steady-state regime ($T_1, T_2 \ll \tau$). In this continuous-wave (cw) regime, all transients have died out, so that u, v, and w are functions of only z and ζ.

C. Coherent regime

In the coherent regime one must use the fully coupled wave (8) and Bloch [(17)–(19)] equations. For $\langle R \rangle$ we combine Eqs. (2), (10), (14), and (15) and find, neglecting terms in D,

$$R(z,t,\zeta) = -\frac{MN}{2}((u+iv) \times \exp\{i[\omega t - kz - \phi(z)]\} + \text{c.c.}) . \tag{20}$$

To obtain the total stress wave, $R(z,t,\zeta)$ must be integrated over the available spectrum of states:

$$R(z,t) = \int R(z,t,\zeta)g(\zeta)d\zeta . \tag{21}$$

Expressions (9) and (21) can be inserted into the wave equation (8) to obtain equations for $e_0(z,t)$ and $\phi(z)$. Following McCall and Hahn[16] and Shiren,[15] we assume that the envelope e_0 is slowly varying compared to a wavelength or period of oscillation, and that $(M/\rho_0 c^2)\,|u+iv|$ is small compared to e_0. Under these assumptions the in-phase and out-of-phase components of (8) can be written as

$$\frac{1}{c}\frac{\partial e_0}{\partial t} + \frac{\partial e_0}{\partial z} = \frac{M\omega N}{2\rho_0 c^3}\int v(z,t,\zeta)g(\zeta)d\zeta , \tag{22}$$

$$e_0\frac{\partial \phi}{\partial z} = \frac{M\omega N}{2\rho_0 c^3}\int u(z,t,\zeta)g(\zeta)d\zeta . \tag{23}$$

In the coherent regime, pulse propagation is described[17] by these first-order linear integral-differential equations coupled with the Bloch equations (17)–(19).

D. Intermediate regime

A much simpler set of equations can be obtained for the intermediate regime by setting $\dot{u}=\dot{v}=0$ to represent complete loss of phase memory. Thus

$$u(z,t,\zeta)=-\frac{Me_0(z,t)}{\hbar}\frac{T_2^2\zeta}{1+T_2^2\zeta^2}w(z,t,\zeta)\ , \tag{24}$$

$$v(z,t,\zeta)=\frac{Me_0(z,t)}{\hbar}\frac{T_2}{1+T_2^2\zeta^2}w(z,t,\zeta)\ , \tag{25}$$

$$\dot{w}(z,t,\zeta)=-\frac{2MI(z,t)}{\rho_0 c^3\hbar^2}\frac{T_2}{1+T_2^2\zeta^2}\times w(z,t,\zeta)-\frac{w(z,t,\zeta)-w_0}{T_1}\ , \tag{26}$$

where we have used the definition of the acoustic intensity $I\equiv\rho_0 c^3 e_0^2/2$. Equation (22) can then be written as

$$\frac{1}{c}\frac{\partial I}{\partial t}+\frac{\partial I}{\partial z}=\frac{IM^2\omega N}{\hbar\rho_0 c^3}\int\frac{T_2 g(\zeta)w(z,t,\zeta)d\zeta}{1+T_2^2\zeta^2}\equiv-\alpha I\ . \tag{27}$$

The absorption coefficient α can be identified[19] as

$$\alpha(z,t,w,\zeta)=-\frac{M^2\omega N}{\hbar\rho_0 c^3}\int\frac{T_2 g(\zeta)w(z,t,\zeta)d\zeta}{1+T_2^2\zeta^2}\ . \tag{28}$$

Two extreme line shapes are interesting. If inhomogeneous broadening is dominant and the input intensity is small, the denominator acts as a δ function and we have

$$\alpha(z,t,w)=-\frac{\pi M^2 n_0\omega w_0(z,t)}{\rho_0 c^3}\ , \tag{29}$$

which is the familiar low-intensity absorption coefficient. If, on the other hand, homogeneous broadening is dominant, $g(\zeta)$ acts as a δ function to yield

$$\alpha(z,t,w,\zeta)=-\frac{M^2\omega}{\hbar\rho_0 c^3}\frac{T_2 Nw(z,t,\zeta)}{1+T_2^2\zeta^2}\equiv-\sigma Nw\ , \tag{30}$$

where we identify σ as the cross section for a single two-level entity interacting resonantly with a pulse which is long compared to T_2 and centered at a frequency ω at a distance ζ from exact resonance:

$$\sigma=\frac{M^2\omega}{\hbar\rho_0 c^3}\frac{T_2}{1+T_2^2\zeta^2}\ . \tag{31}$$

In the homogeneous limit and for $\zeta=0$, Eqs. (19) and (22) therefore reduce to a pair of coupled, linear, first-order differential equations for $I(z,t)$ and $w(z,t)$:

$$\frac{\partial I}{\partial z}=-\frac{1}{c}\frac{\partial I}{\partial t}+\sigma NIw\ , \tag{32}$$

$$\frac{\partial w}{\partial t}=-\frac{2\sigma Iw}{\hbar\omega}-\frac{w-w_0}{T_1}\ . \tag{33}$$

E. Steady-state regime

For small values of $\alpha_0 z$, where α_0 is the low-intensity attenuation of the medium and z the path length, the amplitude e_0 of the pulse is not a strong function of z and propagation effects are correspondingly small. The problem then approximates a (standing-wave) magnetic-resonance experiment with spin-$\frac{1}{2}$ particles. Setting $\dot{w}=0$ in Eq. (26) yields the steady-state population difference

$$w(\zeta)=\frac{w_0(1+T_2^2\zeta^2)}{1+T_2^2\zeta^2+I/I_{cc}}\ , \tag{34}$$

which describes the inversion produced in a homogeneous line centered at a distance ζ from the infinitely narrow exciting spectrum, or equivalently, the inversion produced in a very wide inhomogeneous line by a cw spectrum at fixed frequency. The spectral width of $w(t=\infty,\zeta)$ is

$$\Delta\zeta(\mathrm{FWHM})=2T_2^{-1}(1+I/I_{cc})^{1/2}\ . \tag{35}$$

Equations (34) and (35) exhibit the familiar phenomena of saturation and power broadening for intensities above a critical value

$$I_{cc}=\rho_0 c^3\hbar^2/2M^2T_1T_2\ . \tag{36}$$

Substitution of Eq. (34) into Eq. (28) and integration over ζ leads to $\alpha\propto(1+I/I_{cc})^{-n}$ with $n=1$ for the homogeneously broadened case and $n=\frac{1}{2}$ for inhomogeneous broadening.

We define a critical intensity I_c as the input for which $\alpha=\alpha_0/2$. Thus in the cw limit, $I_c=I_{cc}$ for homogeneous broadening and $I_c=3I_{cc}$ for the inhomogeneous case. Similarly, we define a critical energy density $\mathscr{E}_c=I_c\tau$.

F. Modified rate equations

A rigorous solution in the intermediate regime with inhomogeneous broadening would require a combination of Eqs. (22), (25), and (26) into a pair of integral-differential equations. However, it is possible to modify the much simpler rate equations (32) and (33) and use them to approximate the inhomogeneous case, at least for $I\lesssim I_c$. We modify the

parameters N and σ, taking into account the pulse of finite length τ with a spectral width $\Delta\omega \approx 2\pi/\tau$ [full width at half maximum (FWHM)]. We take the effective number of absorbers to be

$$\bar{N} = hn_0[\tau^{-1} + (2T_2)^{-1}] \tag{37}$$

and, to satisfy the independence of α from τ or T_2 in Eq. (29), we take an effective cross section to be

$$\bar{\sigma} = M^2\omega[\tau^{-1} + (2T_2)^{-1}]^{-1}(\hbar\rho_0 c^3)^{-1} ,$$

in analogy with Eq. (31) for $\zeta = 0$. $\bar{N}$ and $\bar{\sigma}$ are used in place of N and σ in the actual fit to the data in Sec. IV.

G. Power broadening

As in the cw case, power broadening in the intermediate regime undoubtedly scales as T_2^{-1} and is therefore less important the shorter the pulse. Furthermore, power broadening in the intermediate regime is time dependent,[9] and states in the wings of the long-time power-broadened spectrum require a reasonably large fraction of T_1 to respond, especially for input intensities no greater than, for example $10I_c$. Therefore, power broadening in the intermediate regime is observable only near the transition to the cw regime ($\tau \approx T_1$) and is most significant for $T_2 \ll \tau$. In Sec. IV we make quantitative estimates of the importance of power broadening under the present experimental conditions.

H. Spectral diffusion

The dominant contribution to the loss of phase memory at temperatures below 1 K is a particular type of spectral diffusion[20,21] in which the thermal flipping of two-level systems outside the pulse spectrum causes a wandering in energy of the states which are in resonance with the pulse. This interaction occurs through the diagonal coupling in Eq. (2) and produces a spectral width $\Gamma(t,T)$ which depends on *time* as well as temperature. At times short compared with T_1 ($E \approx k_B T$), $\Gamma \propto tT^4$, whereas at much longer times $\Gamma(t,T) \rightarrow \Gamma(\infty,T) \propto T$.

The effect of spectral diffusion on the phase memory as measured by phonon echoes is more drastic. The result is an effective time constant $T_2(\text{pe}) \propto T^{-2}$, in agreement with experiment. Because of the time dependence of this complicated situation, it is not clear which value to assume for the effective T_2 in a single-pulse saturation experiment—Γ^{-1}, or $T_2(\text{pe})$ extrapolated to higher temperatures. As we shall see below, the difference between these two options is fortunately small at the temperatures of interest for the present experiment. We shall assume $T_2 = \beta T^{-2}$ with β to be determined by comparison with the data for I_c.

III. APPROXIMATE SOLUTIONS

A. Analytic limiting cases

The coupled rate equations for the incoherent case, Eqs. (32) and (33), do not have closed-form solutions for $I(z,t)$ and $w(z,t)$. However, we can obtain approximate analytic expressions for certain limiting cases.

For the cw regime ($T_1, T_2 \ll \tau$), equilibrium is attained in a time short compared with τ, so that we may set $\partial I/\partial t = \partial w/\partial t = 0$. The rate equations are reduced to[22]

$$\ln[I(z)/I_0] + \frac{2\sigma T_1}{\hbar\omega}[I(z) - I_0] = \sigma N w_0 z , \tag{38}$$

where I_0 is the input intensity. This equation for $I(z)$ can be solved numerically to obtain the absorption as a function of input intensity and distance, and can also be used to find an expression for I_c:

$$I_c = \frac{\hbar\omega\alpha_0 z}{4\sigma T_1}[1 - \exp(-\alpha_0 z/2)]^{-1} . \tag{39}$$

For a thin absorber ($\alpha_0 z \ll 1$), Eq. (39) simplifies to

$$I_c \approx \frac{\hbar\omega}{2\sigma T_1} . \tag{40}$$

If $\sigma = T_2\omega M^2/\hbar\rho_0 c^3$, we regain the expression for I_{cc}, Eq. (36).

For a thick absorber ($\alpha_0 z \gg 1$), Eq. (39) becomes

$$I_c \approx \hbar\omega\alpha_0 z/4\sigma T_1 . \tag{41}$$

In the intermediate regime ($T_2 < \tau < T_1$), the rate equations have been solved analytically[23,24] for the limiting case of no relaxation ($\tau \ll T_1$), with the results[23]

$$I(z,t) = I_0(t)[1 + (e^{-\sigma N J_z} - 1)e^{-2\sigma J_t/\hbar\omega}]^{-1} , \tag{42}$$

$$w(z,t) = w_0(z)e^{-\sigma N J_z}(e^{2\sigma J_t/\hbar\omega} + e^{-\sigma N J_z} - 1)^{-1} , \tag{43}$$

where J_z and J_t are integrals over distance and time:

$$J_z = \int_0^z w_0(z')dz' \quad \text{and} \quad J_t = \int_0^t I(t')dt' . \tag{44}$$

We can derive an expression for I_c in this regime:

$$I_c = (\hbar\omega/2\sigma J_t)\ln\{(e^{\alpha_0 z} - 1)/[I_0(t)e^{\alpha_0 z/2} - 1]\} , \tag{45}$$

where t refers to the time at which the maximum amplitude occurs.

Equation (45) reduces to

$$I_c \approx \begin{cases} \hbar\omega/2\sigma\tau & \text{for } \alpha_0 z \ll 1 \quad (46) \\ \hbar\omega\alpha_0 z/4\sigma\tau & \text{for } \alpha_0 z \gg 1 \, . \quad (47) \end{cases}$$

The expressions for I_c, Eqs. (40), (41), (46), and (47), may also be derived intuitively if one defines I_c as that intensity which, in the cw regime, excites the states as rapidly as they decay, or, in the intermediate regime, as the intensity which, multiplied by the pulse length, yields sufficient *energy* $\mathscr{E}_c$ to excite only half of the available states.

To simulate our experimental results, we need to calculate pulse shapes, population changes, and the effective attenuation after a complete round trip for a variety of input intensities, pulse lengths, and sample parameters. This can be done using Eqs. (42) and (43) for the pulse regime, but for completeness we have developed a numerical simulation of the rate equations which can be used in all four coherent regimes (thick or thin sample, intermediate or cw) including the crossover regions between the limiting cases.

B. Finite-difference algorithms

In applying the method of finite differences to the rate equations, it is convenient to take forward differences in distance (i) and backward differences in time (k). The results of this approach are

$$w_{i,k} = \frac{w_{i,k-1} + (\Delta t/T_1) w_0}{1 + (2\sigma\Delta t/\hbar\omega) I_{ik} + \Delta t/T_1} \quad (48)$$

and

$$I_{i+1,k} = (1 - \Delta z/c\Delta t - \Delta z \alpha_n) I_{ik} + (\Delta z/c\Delta t) I_{i,k-1} + \Delta z \sigma N w_{i,k} \, , \quad (49)$$

where we have included a term in the rate equations to represent any nonsaturable attenuation α_n that may be present in the experiment.

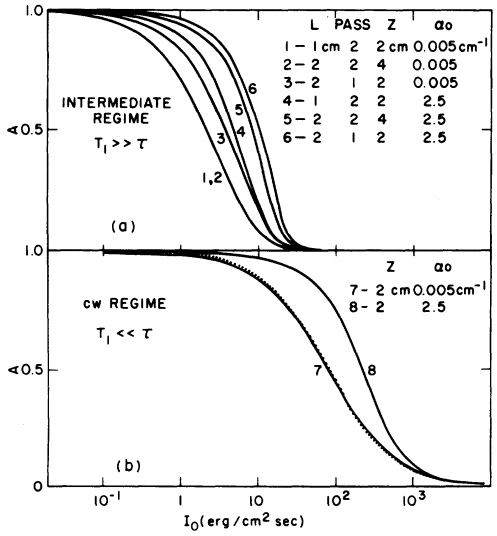

FIG. 1. Normalized effective attenuation $A = \alpha/\alpha_0$, where α_0 is the unsaturated attenuation, as a function of input peak intensity I_0. z is the total path traveled by the pulse. The solid curves are the solution of the rate equations (32) and (33). The dotted curve is $(1 + I/I_c)^{-1}$, with a critical intensity $I_c = 8.17$ erg/cm^{2}sec pulse. Pulse length $\tau = 90$ nsec, sample length $L = 1$ or 2 cm, $f = 0.692$ GHz, and $\sigma = 7.74 \times 10^{-12}$ cm^2.

C. Numerical results

We have used the numerical procedures and analytic expressions described above to explore the behavior of the rate equations in the various regimes of T_1/τ and $\alpha_0 z$ for both a single pass and a round trip through the absorbing medium. These results are general and may be applied to any system in which a pulse (optical or acoustic, for example) is traveling through a saturable, homogeneously broadened medium in either the cw or the intermediate regime. The transition to the coherent case will be discussed below.

The normalized saturation curves in Fig. 1 show the dependence of the absorption on the peak input intensity I_0 after either one or two passes for several extreme cases. While the results are very general, a convenient scale factor for the intensity has been chosen to facilitate comparison with the experimental data. In the intermediate regime [Fig. 1(a)] the effect of the second pass in a thin absorber (curves 2 and 3) is simply to lower I_c by approximately a factor of 2. The probability of any two-level system being excited by the pulse is doubled on the second pass if the pulse is weakly absorbed ($\alpha_0 z \ll 1$). For a thick absorber ($\alpha_0 z \gg 1$), on the other hand, curves 5 and 6 illustrate the competition between the above effect and the dependence of I_c on $\alpha_0 z$ [Eq. (47)]. Equation (46) is consistent with curves 1 and 2 having the same I_c. Curves 4 and 6 compare a two-pass case with a single pass through a sample twice as long (same $\alpha_0 z$). The effect is a shift by again a factor of 2 in I_c. In Fig. 1(b) there is no difference between single and double pass in the cw regime, as expected. Furthermore, the variation as $(1 + I_0/I_c)^{-1}$ is clearly shown for $\alpha_0 z \ll 1$. We note that in both regimes the transition at I_c is broader for small $\alpha_0 z$ than for large $\alpha_0 z$.

The critical intensity I_c extracted from such saturation curves is shown in Fig. 2 as a function of $\alpha_0 z$ and T_1. The transition from one extreme to another is smooth and the numerical calculations

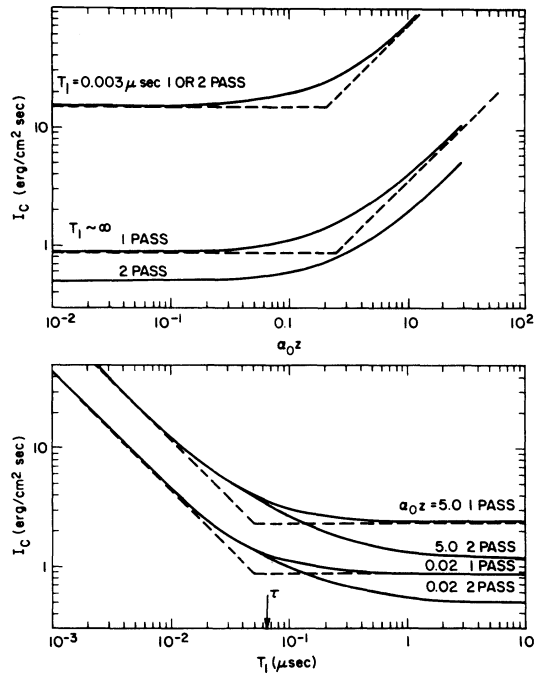

FIG. 2. Calculated values of I_c as a function of $\alpha_0 z$ and T_1. $\sigma = 5.0 \times 10^{-11}$ cm^2, $f = 0.692$ GHz, and $\tau = 65$ nsec. The dashed lines represent the limiting values described in the text.

agree quite well with the limiting cases (dashed straight lines) obtained from Eqs. (40), (41), (46), and (47). The dependence on τ, σ, and ω in these expressions is also reproduced in the numerical results. Variations in I_c on the order of 10% are observed for the two-pass case in the intermediate regime if one uses different input pulse shapes. The general behavior can be visualized with the help of the three-dimensional representation of $I_c(\alpha_0 z, T_1)$ in

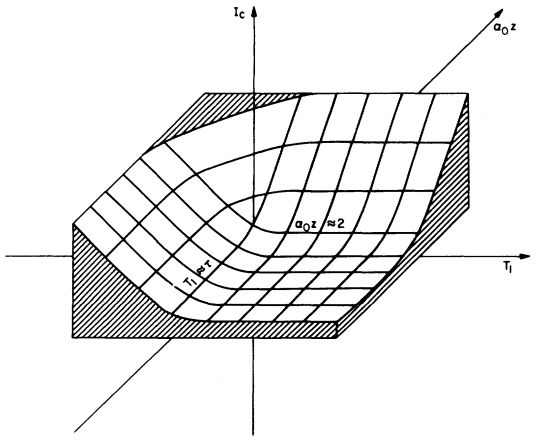

FIG. 3. Surface for I_c $(\alpha_0 z, T_1)$ for a particular value of $\omega/\sigma\tau$ and a single pass. Different values of $\omega/\sigma\tau$ will scale the surface as described in the text.

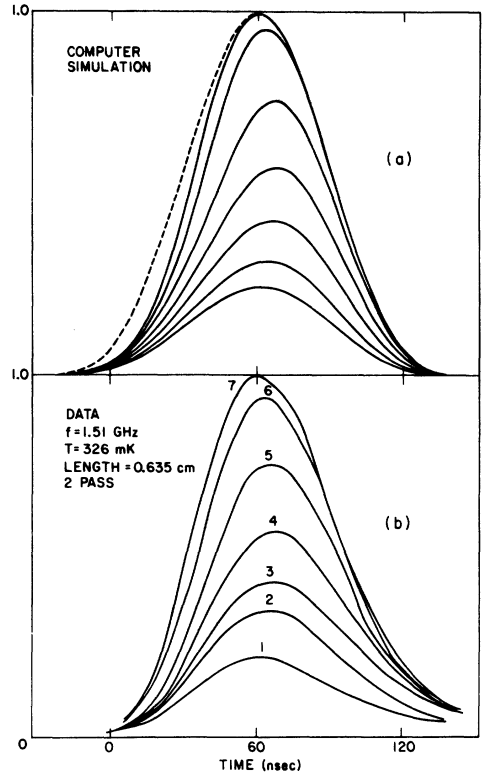

FIG. 4. Pulse shape $I(t)$ after one round trip, normalized to the peak intensity I_0 of the input pulse, for a number of input intensities near I_c. Calculated pulse shapes are shown in (a) for the input pulse (dotted line) and for input intensities $I_0 = 0.19$ (1), 0.48 (2), 0.92 (3), 1.51 (4), 2.59 (5), 5.89 (6), and 11.1 (7), in units of $I_c = 9.55 \times 10^{-7}$ erg/cm^2 pulse. The calculations simulate the conditions of the data (b) for acoustic propagation in fused silica.

Fig. 3. For $T_1 \ll \tau$, I_c scales as $\hbar\omega/\sigma$, whereas for $T_1 \gg \tau$, $I_c \propto \hbar\omega/\sigma\tau$.

For $I_0 \sim I_c$ and $T_1 \gtrsim \tau$, the trailing part of the pulse encounters a medium which has been partially saturated by the leading edge. Significant reshaping of the pulse can occur for large $\alpha_0 z$, as shown in Fig. 4(a). We have used an input pulse shape given by

$$I_{z=0} = I_0 \sin^4(\pi t/2.75\tau) , \tag{50}$$

which has a FWHM equal to τ. It is useful to calculate the FWHM and the time delay of the output pulse as a function of $\mathscr{E}_0 = I_0\tau$ and $\alpha_0 z$ (Fig. 5). Pulse narrowing at large $\mathscr{E}_0$ is due to the leading edge of the pulse being more highly absorbed than the rest. One might have expected a certain amount of pulse broadening for a large $\alpha_0 z$ as a precursor to the extreme broadening found in the coherent regime.[17,25] The absence of pulse broadening in Fig. 5 is probably due to our incomplete treatment of inhomogeneous broadening and phase memory. The

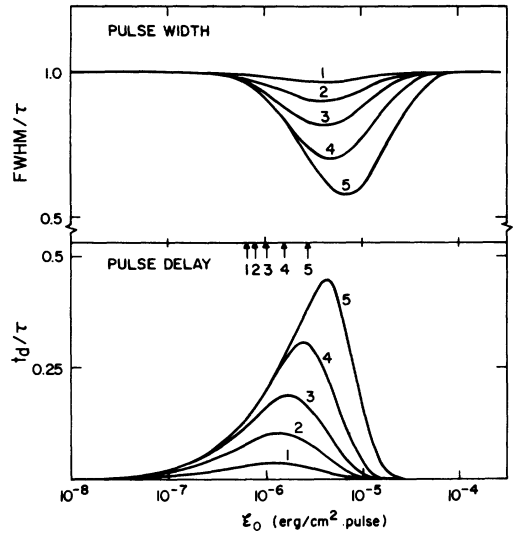

FIG. 5. Calculated pulse width (FWHM) and pulse decay (t_d) as functions of $\mathscr{E}_0$ and of $\alpha_0 z$. Values of $\alpha_0 z$ are 0.5 (1), 1.5 (2), 3.0 (3), 6.0 (4), and 12.0 (5). The five critical energies $\mathscr{E}_c$ are shown by arrows.

maximum amount of pulse delay depends on $\alpha_0 z$ and the shape of the input pulse but has a limiting value of approximately $\tau/2$. This behavior is also in contrast to what is expected for the coherent regime[17,25] but can be understood as described in Sec. IV.

In the cw case a perfectly rectangular pulse undergoes no reshaping, but the leading and trailing edges of a more realistic pulse will be made sharper if I_0 is in the vicinity of I_c. This is because the peak experiences less attenuation (for a typical saturation curve) than the (lower-intensity) leading or trailing edges. The narrowing, however, should produce no pulse delay.

IV. DATA AND ANALYSIS

Measurements of acoustic saturation and the recovery from saturation have been made in conjunction with an investigation of phonon echoes in a glass at low temperatures.[26] Phonon echoes are observable only below $T\sim 0.1$ K for the conditions of our experiment, but the saturation and recovery measurements were continued up to $T\sim 0.5$ K. The technique has been described previously.[26] Most of the data were obtained with pulse length $\tau=65$ nsec at a frequency $f=0.692$ GHz using a ZnO thin-film transducer on a 0.635-cm cube of Suprasil W in contact with a ^{3}He-^{4}He dilution refrigerator. Some of the data were obtained with $f=1.5$ GHz and some with τ up to 500 nsec.

Pulse reshaping is clearly visible in most of the data, especially for large $\alpha_0 z$. An example is shown in Fig. 4(b), where we have emphasized the reshaping by choosing a higher frequency to obtain a large α_0. The experimental pulse shape is distorted by the imperfect transient response of the amplifiers, particularly on the trailing edge, but the qualitative agreement with the computer simulation in Fig. 4(a) is evident.

Saturation data are shown in Fig. 6 for the shortest τ at 0.692 GHz and a number of different temperatures. The solid lines represent the computer simulation with parameters which have been chosen to yield overall best agreement with the data. The agreement with I_c is obtained by choosing $\gamma_L=2.5$ eV. $\bar{N}$ and $\bar{\sigma}$ are calculated with the parameters given in the caption. The unsaturated absorption $\alpha_0 z$ ($I_0 \ll I_c$) agrees with the expected dependence of α_0 on $-w=\tanh(\hbar\omega/2kT)$. The curves in all cases exhibit a somewhat sharper transition at I_c than do the data, but the trend toward a broader transition at the highest temperature is reproduced by the calculation, where it is due to $\alpha_0 z \lesssim 1$.

A closer comparison between the calculated and experimental values of I_c is made in Fig. 7, where a few points for larger τ and lower T have been included. For convenience, we have chosen to plot $\mathscr{E}_c$, the critical energy per cm^2 in each pulse. At the highest temperatures, $\mathscr{E}_c(\tau,T)$ tends toward a simple T^2 dependence, independent of τ, in agreement with Eq. (46) for $\sigma\sim T_2\sim T^{-2}$ in the intermediate regime. If the intermediate regime were retained to the lowest temperatures, the data should follow the

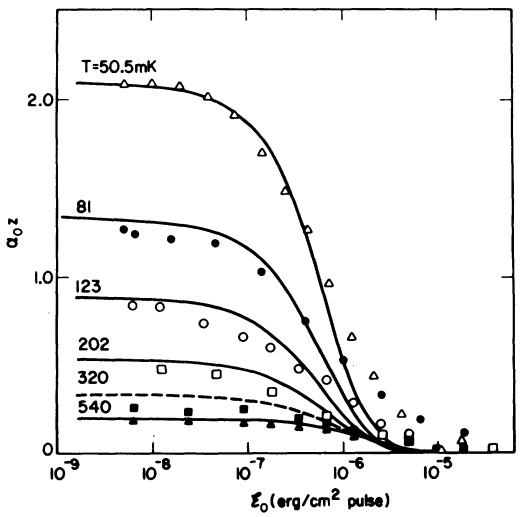

FIG. 6. Attenuation of an acoustic pulse after one round trip in Suprasil W at various temperatures. The lines are fits to the data using the following parameters: $\tau=65$ nsec, $f=0.692$ GHz, $T_2=7\times10^{-3}$ μsec K^2/T^2, $\rho_0=2.2$ g/cm^3, transverse velocity $c_T=5.8\times10^5$ cm/sec, and sample length $L=0.635$ cm.

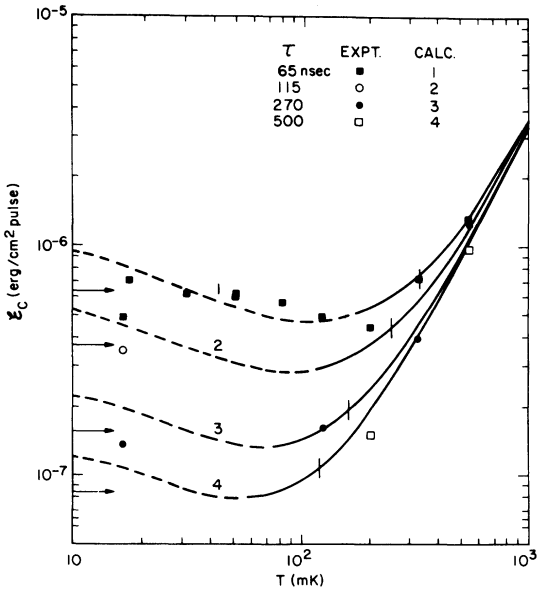

FIG. 7. Critical energy density $\mathscr{E}_c$ vs temperature for the data in Fig. 6 as well as for data obtained with longer pulses and at lower temperatures. The solid-dashed lines are calculated with rate equations using parameters given in the text. The arrows at the lowest temperatures are approximate predictions for the coherent regime (Ref. 17).

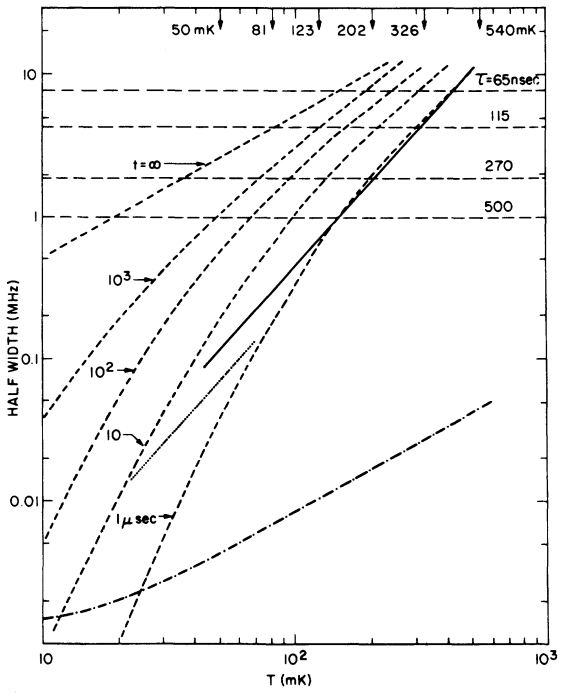

FIG. 8. Temperature dependence of various contributions to the spectral halfwidth. The short-dashed lines are the spectrum of excited states $\Gamma/2\pi$ for various times after excitation, based on calculations of spectral diffusion in Ref. 20. The halfwidth $(2\pi T_2)^{-1}$ due to the phase memory time T_2, as measured with phonon echoes, is plotted with a dotted line. The solid line represents the $T_2(T)$ which is used to fit the data in Figs. 6 and 7. Also shown, with long-dashed lines, are the halfwidths $(2\pi\tau)^{-1}$ of the experimental pulse spectra. $(2\pi T_1)^{-1}$ for $\gamma_L = 2$ eV is plotted for comparison as a dotted-dashed line.

dashed lines which vary as $\alpha_0 \propto \tanh(\hbar\omega/2kT)$. However, the most complete data ($\tau = 65$ nsec) remain roughly constant for $T \lesssim 200$ mK. The disagreement is consistent with the low-temperature data occurring in the coherent regime. The dependence on pulse *length* $\mathscr{E}_c \propto \tau^{-1}$, also agrees with predictions in the coherent regime[16] as indicated by arrows. The transition from the coherent to the intermediate regimes occurs at $T_2(T) = \tau/2$, indicated by vertical lines in Fig. 7. In Fig. 8 we compare the values for T_2 used in the fit with the bandwidth of the pulse. As described in Sec. II H, spectral diffusion in a glass at these temperatures is a time-dependent process and it is not clear which to use as the effective T_2—the phonon echo phase memory time or the inverse linewidth after a time $\sim\tau$. The spectral diffusion width calculated by Black and Halperin[20] has been interpolated from their figures and scaled up as in Ref. 11 to match bandwidth measurements. We see that, in fact, the two choices for the effective linewidth are similar for 0.05 K $< T <$ 0.5 K using a spectral-diffusion time equal to τ, and not very different from the T_2 used in the fit to the I_c data.

As discussed in Sec. II G, power broadening is another time-dependent process that might be important for $\tau \approx T_1$ and $T_2 < \tau$. However, from the calculated behavior of the population spectrum with

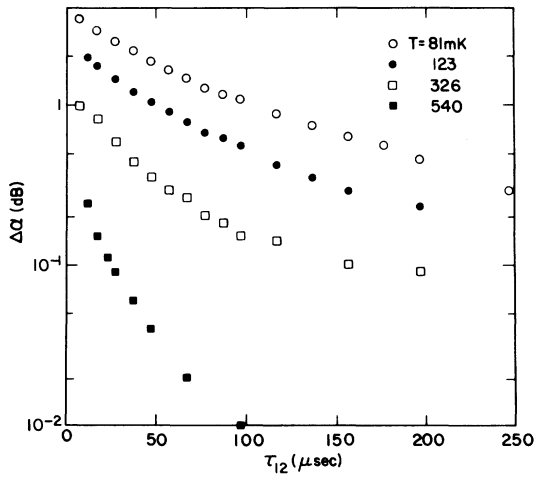

FIG. 9. Change in acoustic attenuation of a weak second pulse caused by a strong first pulse. τ_{12} is the time between pulses. Frequency $f = 0.692$ GHz.

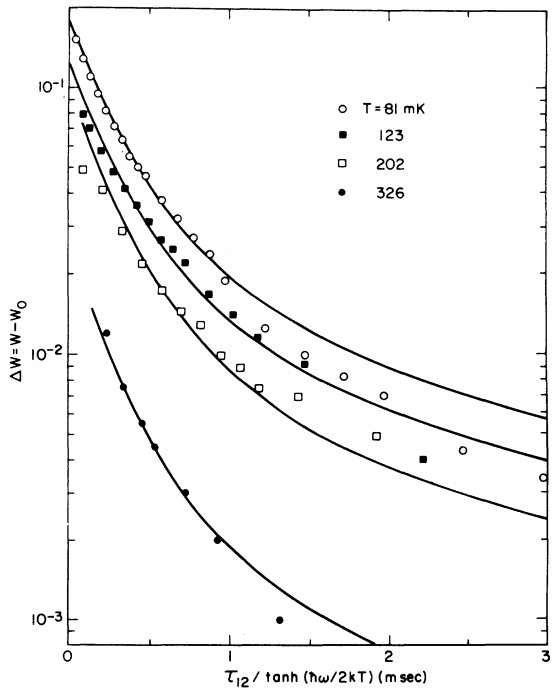

FIG. 10. Recovery of the population w to its equilibrium value w_0 after saturation. The values are obtained from the data in Fig. 9 by means of a rate-equation simulation. The solid curves are fit to the data using $\gamma_L = 1.6$ eV and the distribution function $p'(r)$ described in the text.

time,[9] we estimate for our worst-case parameters (largest τ and smallest T_2) that the power-broadened response is only 10—20% of the long-time value. Thus we feel safe in ignoring the effects of power broadening.

The data presented thus far are obtained with a single pulse. If one uses instead a strong first pulse followed after a time τ_{12} by a weaker second pulse, the apparent attenuation of the second pulse can be used to monitor the recovery of the system from saturation. In principle, this provides a direct measurement of T_1. The results of such a measurement are shown in Fig. 9 for several temperatures. To extract a value of T_1, however, one must first transform changes of attenuation into changes of fractional population difference Δw. The transformation is accomplished by simulating the absorption numerically for the actual intensity of the second pulse as a function of an initial w. Inputs for w in the numerical simulation range from w_0, the value in thermal equilibrium at the experimental temperature, to $w=0$, representing complete saturation. The results of the transformation are plotted as $\Delta w = w - w_0$ in Fig. 10. It is clear that the decay of Δw at any temperature is not exponential. The slope varies by nearly an order of magnitude from the beginning to the end of the data at the lower temperatures. The solid lines are the result of fitting a distribution $p'(r)$ similar to Eq. (6) but with a factor of r^2 instead of r in the denominator. The higher power of r increases the number of slower, asymmetric states relative to the faster, symmetric states.[27] We calculate the decay using the expression

$$\Delta w = w_1 \int_0^1 p'(r) r^2 \exp[-r\tau_{12}/T_1(\min)]dr \ , \tag{51}$$

where w_1 is the initial value of Δw and depends on the strength of the first pulse. The factor of r^2 is due to the fact that the excitation of a particular state by each of the two pulses is proportional to r. This cancels the r^{-2} in $p'(r)$ and keeps the integral finite. Thus the cutoff at small r which is required to keep the total number of states finite cannot be determined from the present fit. The best fit to the data corresponds to $\gamma_L \sim 1.6$ eV. The expression for $p'(r)$ is certainly not unique but yields a much better fit than with, for example, r^{-1} or $r^{-3/2}$ in place of r^{-2}.

Several additional comments about saturation recovery are appropriate. If the intensity of the saturating first pulse is much greater than I_c, it does not fall to a negligible intensity after one round trip but continues to reflect back and forth, resaturating the states until it spreads out by diffraction or is consumed by nonresonant absorption in the sample, reabsorption in the transducer, etc. This effect tends to keep Δw at a higher value than without the multiple passes. For this reason we have chosen saturating pulse intensities which are not much greater

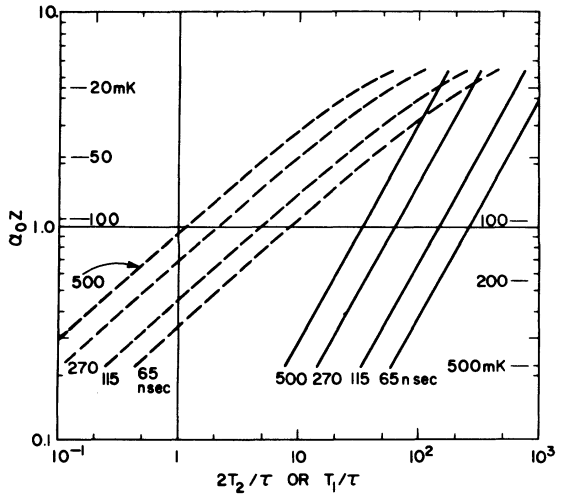

FIG. 11. Location of the data in the $\alpha_0 z - T_1/\tau$ (solid lines) and $\alpha_0 z - 2T_2/\tau$ (dashed lines) planes.

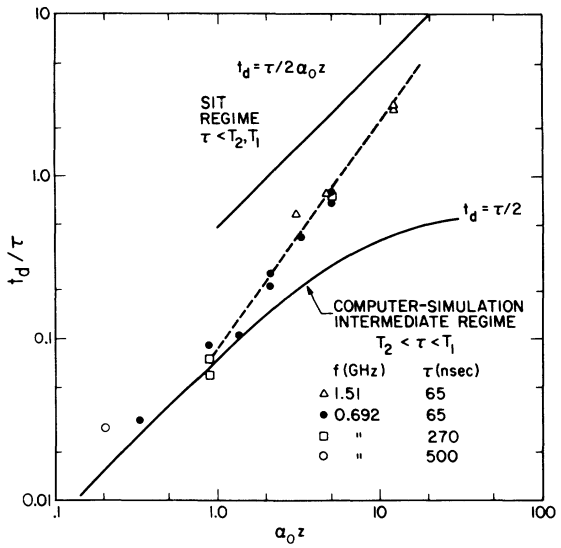

FIG. 12. Maximum delay of the peak of a pulse after one round trip. Zero delay time occurs for either very large or very small pulses, and the maximum delay occurs for $I_0 \sim I_c$. The solid curve is based on rate equations [compare Fig. 5(b)] and the solid straight line on self-induced transparency (SIT).

than I_c. In addition, we have delayed the fit at higher temperatures by three round trips. A competing effect is due to spectral diffusion which takes energy from states at $\omega = \omega_0$ and spreads it over a width $\Delta\omega \propto T$, which can be estimated from the curves in Fig. 8. The effect is significant for $\tau = 65$ nsec only at the highest temperature, but even there the spreading is in the long-time limit after $\tau_{12} \approx T_1$, after which further changes are small compared to the changes observed in Δw. Thus there is some uncertainty in the interpretation of Δw for $\tau_{12} < T_1$, and the fits to the data in Fig. 10 are optimized primarily at later times.

With the above estimates of T_1 and T_2, it is interesting to locate our data in the $\alpha_0 z - T_1/\tau$ or $\alpha_0 z - 2T_2/\tau$ planes (Fig. 11). The data presented above all lie along the lines for the four pulse widths. The boundary between the intermediate and coherent regimes ($\tau \approx 2T_2$) occurs at relatively high temperature ($T \sim 200$ mK for $\tau = 65$ nsec). It is mildly surprising, therefore, that the rate-equation approach works as well as it does, down to $T \sim 50$ mK in Fig. 6, for example. The reason is probably that the transition is very gradual. To examine this transition more closely, we plot the maximum pulse delay as a function of the number of absorption lengths in Fig. 12. For data lying well within the intermediate regime (high temperatures, long pulses), there is agreement with the predictions of the rate equations. For $\alpha_0 z \gtrsim 1$ which occurs at lower temperatures, there is a clear deviation to larger delay, even exceeding τ. This is consistent with a smooth transition to the self-induced-transparency prediction[16] for large $\alpha_0 z$ in the coherent regime, i.e., a decreased pulse velocity with a delay proportional to $\alpha_0 z$. Such behavior occurs when a 2π pulse travels with essentially no loss as the front half of the pulse inverts the two-level systems and the back half stimulates them to return their energy to the pulse, producing a reduced group velocity. The characteristic distance for this process is one absorption length α_0^{-1}, which explains qualitatively why $\mathscr{E}_c(T)$ remains constant in the coherent regime. The path length z in Eq. (47) for I_c might be replaced by α_0^{-1} upon entering the coherent region, thus eliminating the $\alpha_0 z$ dependence which is responsible for the temperature dependence of the rate-equation prediction in Fig. 7.

V. CONCLUSION

The rate equations which describe pulse propagation in the intermediate and cw regimes for a homogeneously broadened line have been used to map out the behavior of the critical intensity and pulse reshaping. The analysis may be applied to any saturable absorber with two-level systems satisfying these conditions.

The present acoustic data occupy the intermediate and coherent regimes at high and low temperatures, respectively. We have used expressions for the homogeneous case which have been modified to represent the spectrum of excited states in an inhomogeneously broadened absorber. With this modification, we obtain a consistent description of the temperature and pulse-length dependence of I_c in the intermediate and, approximately, in the coherent regimes. The coupling constant determined from this fit is $\gamma_L(I_c) = 2.5$ eV. The *shape* of the saturation curves, on the other hand, is not so well described by the rate equations, being in all cases somewhat broader than the calculated curves. This is perhaps due to the neglect of the ζ dependence which appears in Eqs. (22), (25), and (26). It is more likely due to a distribution of matrix elements $p(r)$, because this broadening is also observed in the low-temperature, coherent regime.

We have used the numerical simulation to transform saturation recovery data from changes in attenuation to changes in population. It is clear from the latter that there is a distribution of states with decay times ranging over at least a factor of 10, as expected on a two-level tunneling model. A reasonable description of the shape of the decay curves is obtained with a distribution function which emphasizes the slower, asymmetric states.

From this fit we determine γ_L (sat. rec.) ≈ 1.6 eV.

A reanalysis of the phonon echo data using a similar distribution of coupling strengths leads to $\gamma_L(\text{pe}) \approx 2.0$ eV. Thus our best estimate is an average of the three results, $\bar{\gamma}_L = 2.0$ eV. We conclude that we are observing the one-phonon decay process in the saturation recovery data. Our pulse lengths are short enough and the temperatures are low enough that neither spectral diffusion nor power broadening is a dominant effect, as they were in previous measurements[28] at higher temperatures with longer pulses.

We have included data at lower temperatures to demonstrate that there is a smooth transition between the intermediate and coherent regimes. This is seen in the temperature dependence of I_c as well as the pulse decay. At the higher values of $\alpha_0 z$, a gradual trend is observed toward self-induced transparency, the characteristic mode of propagation in the coherent regime.

[1]P. W. Anderson, B. I. Halperin, and C. M. Varma, Philos. Mag. 25, 1 (1972).

[2]W. A. Phillips, J. Low Temp. Phys. 7, 351 (1972).

[3]R. C. Zeller and R. O. Pohl, Phys. Rev. B 4, 2029 (1971).

[4]*Amorphous Solids: Low Temperature Properties,* edited by W. A. Phillips (Springer, Berlin, 1981).

[5]S. Hunklinger, W. Arnold, S. Stein, R. Nava, and K. Dransfeld, Phys. Lett. 42A, 253 (1972).

[6]B. Golding, J. E. Graebner, B. I. Halperin, and R. J. Schutz, Phys. Rev. Lett. 30, 223 (1973).

[7]C. P. Slichter, *Principles of Magnetic Resonance,* 2nd ed. (Springer, Berlin, 1980), Vol. 1.

[8]M. Sargent, M. O. Scully, and W. E. Lamb, Jr., *Laser Physics* (Addison-Wesley, Reading, 1974).

[9]L. Allen and J. H. Eberly, *Optical Resonance and Two-Level Atoms* (Wiley, New York, 1975).

[10]S. Hunklinger and M. v. Schickfus, in *Amorphous Solids: Low Temperature Properties,* Ref. 4, Chap. 6.

[11]B. Golding and J. E. Graebner, in *Amorphous Solids: Low Temperature Properties,* Ref. 4, Chap. 7.

[12]B. Golding, J. E. Graebner, and R. J. Schutz, Phys. Rev. B 14, 1660 (1976).

[13]J. E. Graebner and B. Golding, Bull. Am. Phys. Soc. 24, 493 (1979).

[14]J. Jäckle, Z. Phys. 257, 212 (1972).

[15]N. Shiren, Phys. Rev. B 2, 2471 (1970).

[16]S. McCall and E. Hahn, Phys. Rev. 183, 457 (1969).

[17]F. A. Hopf, Phys. Rev. A 2, 195 (1970).

[18]J. Joffrin and A. Levelut, J. Phys. (Paris) 36, 811 (1975).

[19]α is defined in analogy with the simple Beers law describing exponential decay, even though the decay for $I_0 \sim I_c$ is not exponential (Ref. 6). We use the operational definition $\alpha = \ln[I(\text{in})/I(\text{out})]$ with I measured at the peak of the pulse.

[20]J. L. Black and B. I. Halperin, Phys. Rev. B 16, 2879 (1977).

[21]P. Hu and L. R. Walker, Solid State Commun. 24, 813 (1977).

[22]F. Gires and F. Combaud, J. Phys. (Paris) 26, 325 (1965).

[23]L. M. Frantz and J. S. Nodvick, J. Appl. Phys. 34, 2346 (1963).

[24]A. C. Selden, Br. J. Appl. Phys. 18, 743 (1967).

[25]I. M. Asher, Phys. Rev. A 5, 349 (1972); R. E. Slusher and H. M. Gibbs, *ibid.* 5, 1634 (1972); 6, 1255(E) (1972).

[26]B. Golding and J. E. Graebner, Phys. Rev. Lett. 37, 852 (1976); J. E. Graebner and B. Golding, Phys. Rev. B 19, 964 (1979).

[27]B. Golding, J. E. Graebner, A. B. Kane, and J. L. Black, Phys. Rev. Lett. 41, 1487 (1978).

[28]S. Hunklinger and W. Arnold, in *Physical Acoustics,* edited by W. P. Mason and R. N. Thurston (Academic, New York, 1976), Vol. 12.